

Delocalization Assisted Transport through Nucleic Acids in Molecular Junctions

Jesús Valdiviezo,^{a,†} Caleb Clever,^{b,†} Edward Beall,^b Alexander Pearse,^c Yookyung Bae,^c Peng Zhang,^{a,*} Catalina Achim,^c David. N. Beratan,^{a,d,e,*} and David H. Waldeck^{b,*}

^aDepartment of Chemistry, Duke University, Durham, North Carolina 27708

^bDepartment of Chemistry, University of Pittsburgh, Pittsburgh PA 15260

^cDepartment of Chemistry, Carnegie Mellon University, Pittsburgh PA 15213

^dDepartment of Physics, Duke University, Durham, North Carolina 27708

^eDepartment of Biochemistry, Duke University, Durham, North Carolina 27710

* Authors to whom correspondence should be addressed: peng.zhang@duke.edu, david.beratan@duke.edu, dave@pitt.edu,

† These authors contributed equally to this work.

ABSTRACT

Charge flow through molecules is central to the function of supramolecular machines, and charge transport in nucleic acids is implicated in molecular signaling and DNA repair. We examine electron transport through nucleic acids to understand the interplay of resonant and non-resonant charge carrier transport mechanisms. This study reports STM break-junction measurements of peptide nucleic acids (PNAs) with a G-block structure and contrasts the findings with previous results for DNA duplexes. The G-block PNA duplexes display a much higher conductance than the corresponding DNA duplexes of the same sequence, however they do not display the strong even-odd dependence conductance oscillations found in G-block DNA. Theoretical analysis finds that the conductance oscillation magnitude in PNA is suppressed because of the increased electronic coupling interaction between G-blocks in PNA and the stronger PNA – electrode interaction compared to that in DNA duplexes. The strong interactions in the G-block PNA duplexes produce molecular conductances as high as 3% G_0 , where G_0 is the quantum of conductance, for duplexes of 5 nm length.

INTRODUCTION

Charge transport through nucleic acids¹⁻¹² can proceed by tunneling, resonant, near-resonant, or incoherent pathways that are sensitive to the macromolecular structure and its environment.¹³⁻¹⁶ Until recently, charge transport through nucleic acids was believed to proceed by coherent tunneling at shorter distances and incoherent (multi-step) hopping at longer distances.^{11, 17-19} However, recent studies found that neither the coherent nor the incoherent pictures are adequate to describe the transport at short to intermediate distances.²⁰⁻²² For example, the single-molecule conductances measured for deoxyribonucleic acid (DNA) duplexes with alternating cytosine (C) and guanine (G) bases, namely $-(GC)_n-$ with n ranging from 3 to 8, were compared to those for duplexes of the same length with the G and C bases separated into blocks, i.e., $-G_nC_n-$.²¹ The $-(GC)_n-$ duplex conductance decreases linearly with n , while the $-G_nC_n-$ (G-block) duplex conductance oscillates with n . The linear decrease of the conductance in $-G_nC_n-$ is consistent with an incoherent charge-transport mechanism. The G-block conductance oscillations suggest extended carrier delocalization (coherence) over strongly-coupled, adjacent G-blocks.²³

The strong sequence dependence conductance found for DNA⁷ and charge transfer²⁴⁻²⁸ indicate sequence-dependent delocalization characteristics. Indeed, the more rapid exponential decrease of electrical conductance in AT duplexes compared to GC duplexes is well documented.²⁹ Less well understood is the influence of cross-strand couplings on the strength and mechanism of nucleic acid charge transfer and transport.³⁰ For example, positioning the molecule-electrode linker groups and the G-blocks on the 3' termini of the DNA duplexes causes an order of magnitude increase in the single molecule conductance compared to duplexes with the electrode-molecule linkers and G-blocks on the 5' termini. This enhancement of the 3'-anchored G-block duplexes was explained by the larger cross-strand G-to-G coupling between G-blocks accessed in the middle

of the 3'-3' structure, compared to the corresponding cross-strand coupling in the 5'-5' chains.³⁰ Because the G-blocks mediate the charge flow,²⁴ the cross-strand block-to-block coupling is critical.³¹ Indeed, the G-to-G cross-strand coupling is estimated to be two to three times larger in the 3'-anchored duplexes than in the 5'-anchored species.³² The amplitude of the even-odd conductance oscillations in the 5'-anchored G-block systems are larger, as a percentage of the total conductance, because the cross-strand coupling is weaker.

Comparing the molecular conductance through aminoethylglycine peptide nucleic acid (PNA) and DNA duplexes with the same base sequences can help to reveal the structural origins of the molecular conductances.³³⁻³⁶ PNA and DNA duplexes that have the same number of bases and the same sequence, but a different backbone structure, can display conductances that differ by 10- to 20-fold.³⁶ These conductance differences were explained as arising from differences in the populations of strongly coupled nucleobases, as well as by differences of energy level broadenings. Indeed, energy level broadening can produce mechanisms that are neither purely coherent nor incoherent. The 'flickering resonance' mechanism,³⁷ relies on accessing conformations through molecular fluctuations that can support coherent transport during the persistence time of the quasi-degenerate energy configurations. The studies reported here describe the single-molecule conductance of G-block PNA duplexes for five different lengths ($n = 3 - 7$), and compare the conductances to those measured in G-block DNA duplexes reported previously.³⁰ This study explores how changes in backbone chemistry influence the conductance values and the relative contributions of coherent and incoherent transport mechanisms.

The structure of N-linked PNA is shown in Figure 1. An amine-modified thymine nucleobase is positioned at the N-terminus of the self-complementary G-block PNA oligomer; Watson-Crick hybridization of the PNA oligomer leads to a PNA duplex that has a palindromic

sequence with amine-modified thymine on both ends of the duplex. Electronic coupling occurs between the electrode and the amine-modified thymine at the N-terminus of one strand of the duplex; the modified thymine at the N-terminus of the complementary strand interacts with the STM break junction tip (N-to-N transport). The N-terminus of PNA is analogous to the 5' terminus of DNA.³⁸ The conductance measured for the G-block PNA duplexes is as much as 20 times larger than is measured for the analogous G-block DNA duplexes, and the even-odd conductance oscillations are found to be less pronounced in PNA.

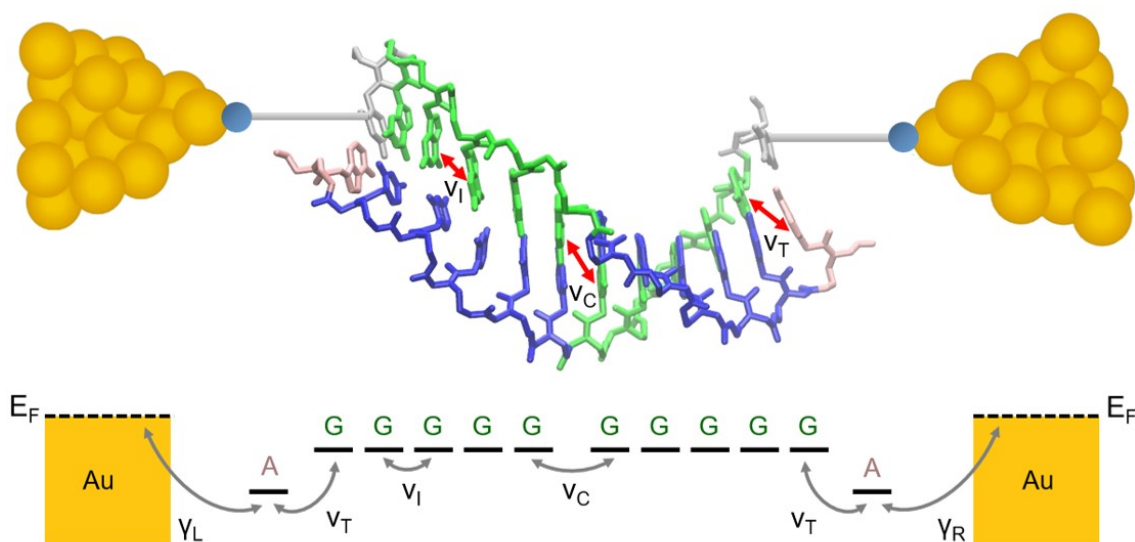


Figure 1. Top: The opposing termini orientations are shown for the N-linked PNA for $n = 5$. The sequence shown is TG₅C₅A and each color represents a different nucleotide. The duplexes are anchored to gold electrodes via amine modifications on the terminal thymine nucleobase. The arrows indicate the nucleobases considered for the GC-GC intra-strand (V_I), GC-GC cross-strand (V_C), and terminal AT-GC (V_T) electronic coupling calculations. **Bottom:** One-dimensional model used in this work. E_F is the Fermi level of the gold electrode, γ_L and γ_R are the molecule-lead electronic couplings, and V_I , V_C and V_T are the nucleobase electronic couplings described above.

The enhanced conductance of PNA duplexes, found in earlier comparisons between DNA and PNA homoduplexes, was attributed to the greater backbone structural flexibility in PNA.³⁶ The current study shows that the conductance of G-block PNA is larger than in G-block DNA, however the G-block duplexes of DNA and PNA appear to have similar structural flexibility (*vide*

infra). Nevertheless, the theoretical analysis suggests that the structural changes associated with the different nucleic acid backbones affect the electronic couplings through the π -stack and the nucleic acid-electrode interactions, producing stronger electrode-molecule coupling for PNA compared to DNA. That is, the electronic coupling interactions near the chain ends (γ_L , γ_R , and V_T , indicated in the middle panel of Figure 1), are much larger for PNA duplexes than for DNA duplexes. The measured conductance value trends for the three duplex types, and the magnitude of the even-odd conductance oscillations are rationalized using an orbital model to describe the mediating state (*vide infra*).

EXPERIMENTAL AND COMPUTATIONAL METHODS

Conductance measurements

Single-molecule conductances were measured for PNA duplexes of different lengths tethered at the N-chain ends. A diffuse duplex monolayer was formed on a gold substrate by spontaneous adsorption from a Tris/EDTA buffer solution of nucleic acid with amine linkers attached to the terminal thymine nucleobases. The electrical conductance of nucleic acid duplexes trapped in a junction between the STM tip and the gold substrate was measured using an AC-modulated scanning tunneling microscope break junction (STM-BJ) method.^{39, 40} This experiment drives the STM tip to the surface of the gold substrate and then withdraws it, allowing molecular junctions to form between substrate and tip. During each tip withdrawal, a triangular voltage waveform is applied between the STM tip and the substrate and a set of current-time profiles are collected. Figure 2 shows an example of a single time trajectory for an STM-PNA-substrate junction, in which the PNA is a sequence of 12 nucleobase pairs. In this experiment, the STM tip is retracted at a rate of 0.1 nm/ms as the bias voltage is modulated with a 2 ms period. The retraction

rate was chosen to balance stability and duration of the molecular junctions. The total length of the trajectory in Figure 2 is about 4 nm. Note the sharp change in current levels near the 640 ms time point. This change is indicative of two distinct junction geometries, and they are described extensively in previous reports.^{29, 36, 40} Conductance measurements on duplex DNA were performed in mesitylene, and values were compared to earlier measurements in buffer solutions.³⁰ Good agreement among the measurements was found, suggesting no significant changes in the conformations of the nucleic acids. For this reason, and for reasons of experimental convenience, conductances were measured in mesitylene solution. Fitting these current-time profiles using a circuit model allows the molecular conductance G to be extracted from the data, and these values are used to build conductance histograms (see Supporting Information).⁴¹ Note that background conductance histograms were also measured in experiments without PNA molecules present. It has been reported that molecular junctions of mesitylene produces conductance values of approximately 0.03 and 0.1 G/G_0 .^{42, 43} However, the length of these junctions is very short, about 0.2 nm, which corresponds to a single voltage modulation period in our measurement (see Figure 2), and it is rejected by our criterion that the molecular junction must persist for at least 4 voltage modulation periods at a consistent current level to indicate a nucleic acid molecular junction. Therefore, any mesitylene conductances that are recorded would be significantly less prevalent than the nucleic acid junctions, as is shown by control experiments; see the Supporting Information for more detail.

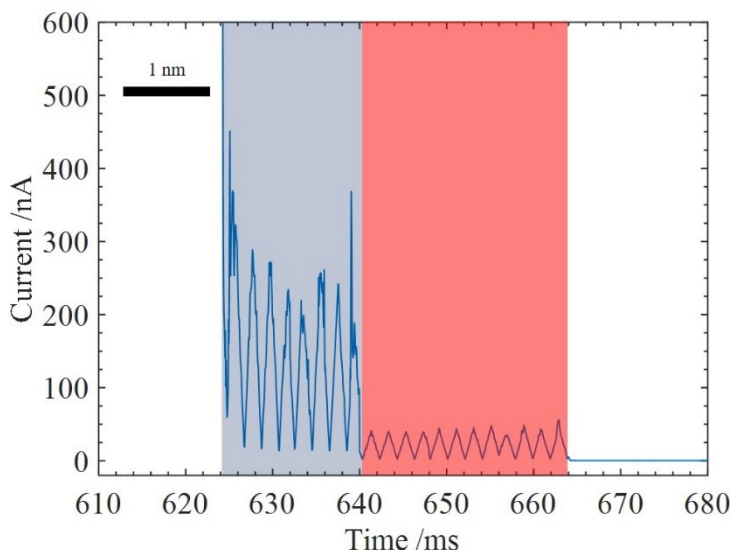


Figure 2. Example current–time $I(t)$ trajectory of a PNA 12-mer G-block molecular junction is shown. Each triangular period is 2 ms in duration, the STM tip retracts by 0.2 nm during each current response period, and the bar shown in the upper left gives the length scale. The initial region (blue) corresponds to the high conductance mode, while the later region (red) is the lower mode. Note that the junction persists for approximately 4 nm, which corresponds to the full length of the PNA molecule.

Molecular dynamics simulations

Nucleic acid conformations were sampled using classical molecular dynamics (MD) simulations, and the structures provide a starting point to compute the energies of specific base orbitals and their electronic coupling interactions. Initial B-DNA structures were obtained using the Avogadro DNA builder tool,⁴⁴ and PNA duplexes were generated with the Schrödinger Maestro molecular modeling software,⁴⁵ starting from a right-handed PNA crystal structure with a heterogeneous sequence (PDB ID: 3MBS).⁴⁶ The CHARMM36 force field DNA parameters,⁴⁷ and the recently developed PNA parameters,⁴⁸ were used (the new PNA force field produces structural ensembles that are consistent with those found using other force fields use in earlier studies).³⁶ The structures were solvated in a TIP3P water box⁴⁹ that extended at least 15.0 Å from each atom. A distance constraint is added between the terminal base-pairs to prevent fraying.⁵⁰ The NAMD 2.11 software⁵¹ was used to run the MD simulations. After energy minimization and

equilibration, the solvated structures were subjected to 100 ns of MD simulation at 300K and 1 atm pressure. Snapshots for each system were saved every 33 ps (3000 coordinate snapshots in all). A detailed description of the procedure is found in the Supporting Information.

Electronic coupling and site energy analysis

For each MD snapshot, the nucleobase HOMO energies and nearest-neighbor cross-strand (V_C), intra-strand (V_I), and terminal AT-GC (V_T) couplings (Figure 1) were computed from the Fock matrix using the block diagonalization method;⁵² the Fock matrix was obtained at the INDO/S level⁵³ from the CNDO program.⁵⁴ The INDO/S method gives a good description of charge transfer parameters in organic π -stacks at a reasonable computational time.⁵⁵ Electronic couplings were computed in the two-state approximation. Only the nucleobases were included in the computation of orbital energies and electronic couplings, denoted as *in vacuo* (solvent and backbone atoms were removed, and dangling bonds were capped with hydrogens). The explicit treatment of backbone and solvent as classical point charges (QM/MM scheme) has been reported to have a small influence on the HOMO energy mean values,⁵⁶ and in sequences with longer bridges, as in this study, the rate constant for hole transfer calculated using a QM/MM formalism and *in vacuo* approaches are similar.⁵⁷ It has also been shown that QM/MM calculated electronic couplings are similar to the *in vacuo* results,^{56, 57} so we used the *in vacuo* results in the analysis described here. The methods used here were shown to provide reliable estimates of the electronic couplings in DNA.^{32, 33}

A cross-strand coupling via the superexchange guanine-cytosine-guanine pathway was also calculated for snapshots taken every 5 ns, using only the four nucleobases in the cross-strand region. A density functional theory approach was selected to describe the hydrogen bonding interactions between nucleobases,⁵⁸ which are relevant for the superexchange pathway. The Kohn-

Sham matrix obtained with the M11 functional⁵⁹ and the ma-def2-TZVPP basis set⁶⁰ as implemented in Gaussian 16⁶¹ was used to compute the associated electronic couplings.

RESULTS AND DISCUSSION

PNA duplex conductance.

Conductance histograms for the N-to-N linked PNA duplexes with the TG_nC_nA sequence ($n = 3 - 7$) are shown in Figure 3, and the most probable conductance for each mode is reported in Table 1. All conductance histograms have two peaks, similar to the histograms reported for other PNA duplexes.³⁶ The multiple peaks in the molecular-conductance histograms were assigned to distinct ‘conductance modes’ that can arise from different binding modes of the linkers and the gold atoms of the surface, specifically the number of gold atoms bonded to the linker, or from different conformations of the molecular junctions.^{62, 63} The contribution of higher conductance modes increases with duplex length. This correlation is consistent with the experimental observation that shorter duplexes, which have lower thermal stability, have shorter average residence times in the junction.²⁹ Thus, the increased statistical weighting of the high conductance mode likely indicates an increased fraction of more stable π -stacked duplexes in the junction, arising from the presence of stronger π overlap between the GC pairs that make the structure more rigid. A more detailed discussion of the different ‘conductance modes’, as well as transitions between them (see Figure 2) and how they are distinguished by the length of time a molecule remains in the junction, is provided in references 29 and 40.

Although both modes are shown in Figure 3, the analysis and discussion focuses on the highest conductance mode in order to draw comparisons with the earlier G-block DNA studies which focused on the highest conductance modes. In some instances, most notably for $n = 4$, a

shoulder or second peak appears at twice the conductance value of the most probable peak for a given conductance mode. This feature was analyzed previously, as well, and is attributed to two or more molecules forming in a molecular junction.^{29,40} In contrast to earlier STM break-junction studies of PNA in which the conductance was well below $10^{-3} G_0$, the G-block duplexes studied here have conductances that are a few percent of G_0 . Measurements at these higher conductances created the need to distinguish molecular signals from background signals arising from (sub)oxide formation on the substrate which appear at $\sim 0.1 G_0$. The measurement protocols and control experiments used to distinguish the two signals are described in the Supporting Information. The conductance shoulders of the histograms in Figure 3 and the (sub)oxide signal were excluded in the Gaussian fitting.

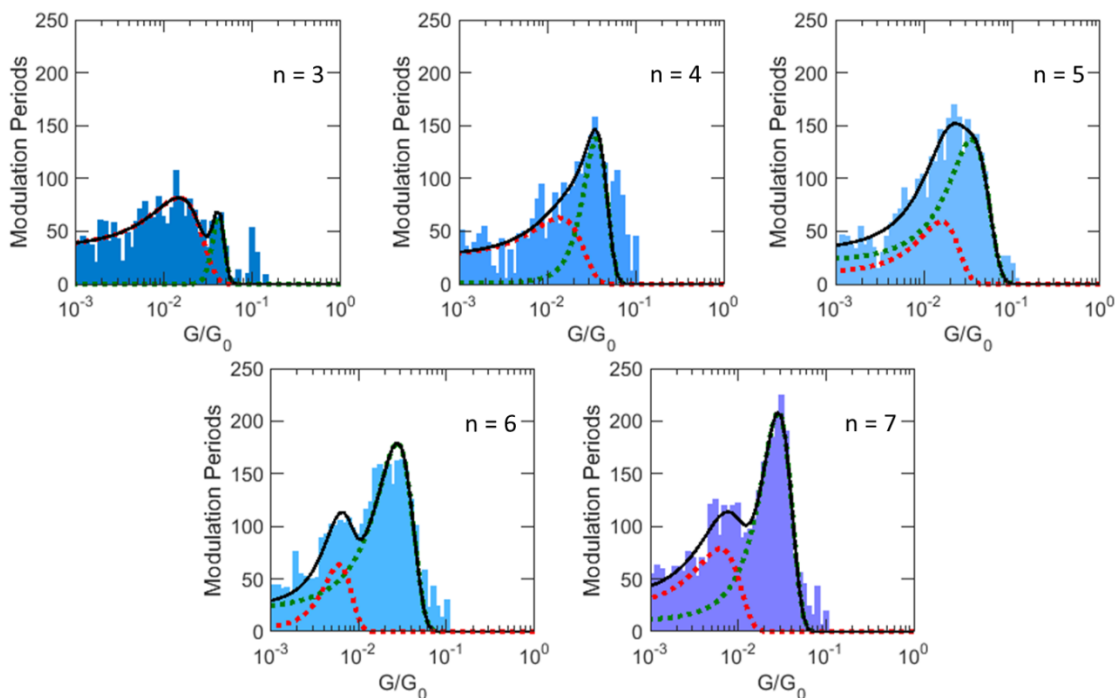


Figure 3. Conductance histograms for the N-to-N linked PNA for $n = 3 - 7$. The black curve is a sum of two Gaussian functions. The dotted red and green curves are the individual Gaussians for the low and high conductance modes respectively. The y-axis shows the number of modulation periods measured.

The average single-molecule conductance for the high-conductance mode shows a modest decrease as the duplex length increases; see Table 1. The influence of the background signal on the measurements is negligible for the $n = 4$ to 7 duplexes, but may contribute to the $n = 3$ measurement, since fewer molecular junctions were sampled in this case (given the decreased residence time of the duplex in the junction). To account for these signal-to-noise constraints, more extensive background measurements were performed, and the peak at $\sim 0.1 G_0$ was excluded from the analysis (see Supporting Information). Note that Table S1 provides a listing of the conductances and standard deviations for the lower conductance mode.

Table 1. The average conductance of the highest observable mode, G , and the standard deviation, σ_G , from the Gaussian fits are shown for the N-linker PNA duplexes for lengths $n = 3 - 7$.

n	$G/G_0 (\times 10^{-2})$	$\sigma_G/G_0 (\times 10^{-2})$
3	4.2	0.6
4	3.6	1.0
5	3.5	1.8
6	2.8	1.4
7	2.9	1.2

The conductances of the $-(G_nC_n)-$ PNA duplexes shows a nearly monotonic, albeit weak, decrease as n increases. Figure 4 plots these PNA data and the conductance data for 3'-DNA G-blocks and 5'-DNA G-blocks. We measured molecular conductances for $n = 3 - 5$ G-blocks of 3' and 5' DNA duplexes (see Supporting Information) and found good agreement with the values reported earlier by Tao and coworkers.^{21, 30} Both of these data sets, the sets reported here and by Tao, are plotted in Figure 4. These data highlight the significant difference in the average conductance for the three duplex types, as well as the decreasing prominence of the conductance variations with even and odd G-block lengths in the three duplexes (see Supporting Information for plots showing the lower conductance modes).

Theoretical analysis of DNA and PNA structure and electronic properties

Molecular dynamics simulations of PNA and DNA duplexes $-(G_5C_5)-$ were run for 100 ns. This time range allows sampling of the inter-nucleobase fluctuations and a subset of duplex conformational changes.³³ Analysis of these structural data indicates that the root-mean square deviations (RMSD) for the structural fluctuations of PNA duplexes are comparable to those of the DNA duplexes. The duplex RMSD value from its average structure calculated with VMD⁶⁴ is 1.3 ± 0.3 Å for N-linked PNA, 1.4 ± 0.4 Å for 3'-linked DNA, and 1.5 ± 0.4 Å for 5'-linked DNA. The small difference in RMSD values suggests that the PNA duplexes are slightly more rigid than the corresponding DNA structures (see Figure S5 and Figure S6). This result is the opposite of results that were found earlier for PNA and DNA duplexes with a *mixed* nucleobases sequence. (For mixed sequences, the PNA duplexes were found to be more flexible than the DNA duplexes.³³) This finding indicates that the relative structural flexibility of the nucleic acids is sequence dependent. The larger overlap between nucleobases in the PNA G-blocks leads to stronger π - π interactions and decreased flexibility as compared to the earlier mixed nucleobase sequence studies of PNA duplexes.⁶⁵

MD snapshots were used to calculate HOMO energy fluctuations for each base pair in the duplexes (at the INDO/S level). The HOMO energy fluctuations and standard deviations of each base pair are shown in Table 2 for the $n = 5$ length, which is illustrated in Figure 1, for the case of PNA. The similar HOMO energies, and their standard deviations suggest that the energy fluctuations are similar for PNA and DNA duplexes. These HOMO energies, calculated *in vacuo*, are 1.5 eV to 2 eV below the Au work function. However, the influence of a metal electrode on the electronic state energies of adsorbed species can be substantial (circa 1 eV⁶⁶), and we expect

the energy offset between the Fermi level and the effective HOMO orbital energies to be significantly less than 1.5 – 2 eV.

Table 2. HOMO energies (eV) and their standard deviations for the GC base pairs examined in the cross-strand, intra-strand, and terminal electronic coupling calculations. These values are computed for $n = 5$ chains.

	DNA 5'		DNA'3		PNA N-end	
	E_{HOMO}	σ	E_{HOMO}	σ	E_{HOMO}	σ
Cross	-6.51	0.22	-6.55	0.21	-6.97	0.19
Intra	-6.41	0.22	-6.37	0.21	-6.47	0.19
Term	-6.68	0.21	-6.71	0.22	-6.56	0.18

We calculated the nearest-neighbor root mean square electronic couplings (V_{RMS}) between base pairs (INDO/S, block diagonalization method, capped bases),³² where $V_{\text{RMS}} = \sqrt{\langle V^2 \rangle} = (1/n) \sqrt{\sum_{i=1}^n V_i^2}$, $V_{\text{RMS}}^2 = \langle V \rangle^2 + \sigma^2$, σ is the standard deviation of V , and n is the number of MD snapshots used for averaging. Table 3 shows the calculated V_{RMS} values. Table 3 reports the calculated electronic couplings of the terminal AT base pairs with their nearest GC pair (V_T) for each of the three duplex types. These calculations indicate a nearly three-fold increase in V_T for N-terminal PNA compared to the corresponding couplings in the DNA duplexes. Table 3 also shows that the N-linker PNA duplex intra-strand couplings (V_I) are larger than the values found for the DNA counterpart. The increase in the couplings, V_I and V_T , for PNA versus DNA are consistent with the larger molecular conductances that are observed experimentally. The cross-strand coupling (V_C) also affects the conductance and earlier work³⁰ showed that it affects the even-odd oscillations and they are discussed next. A description of how these computed electronic coupling values are linked to the conductance measurements follows this subsection.

Table 3. V_{RMS} values of GC-GC cross-strand (V_C), GC-GC intra-strand (V_I) and terminal AT-GC coupling (V_T) in eV. The cross-strand GC-GC couplings for the superexchange pathway (V_C^{SE}) are also shown.

	DNA 5'	DNA 3'	PNA N-end
V_T	0.011	0.017	0.047
V_I	0.087	0.071	0.120
V_C	0.006	0.012	0.002
V_C^{SE}	0.001	0.005	0.017

The direct cross-strand couplings V_C of the N-linked PNA and 5'-linked DNA are both small compared to the other couplings, presumably because of the small overlaps between the G-bases on the two strands (Figure S7). Thus, we examined how these values compared with coupling obtained from a superexchange pathway involving three nucleobases, V_C^{SE} (Table 3). MD simulations show that the geometrical parameters of PNA produce larger G-C π overlaps in the cross-strand region and, as a consequence, stronger π couplings compared to the case in DNA (see Figure S8). The strong π interaction between the stacked GC nucleobases in PNA provides a superexchange pathway for charge transfer. The cross-strand coupling, V_C^{SE} for the guanine-cytosine-guanine superexchange pathway was calculated for selected snapshots taken every 5 ns with density functional theory to describe hydrogen bonding interactions (M11/ma-def2-TZVPP, block diagonalization, capped bases).^{58, 67} $V_C^{SE} = V_{G5-C6}V_{G6-C6}/\Delta E$, where the subscripts indicate the nucleobase and the position in the $n = 5$ duplex (see Figure S10). and ΔE is the energy difference between guanine and cytosine localized states, which is close to 0.7 eV.^{68, 69} V_C^{SE} , which are the RMS couplings, are included in Table 3. V_C^{SE} is larger than the RMS V_C values only for PNA, suggesting that the superexchange contribution to the cross-strand coupling is more relevant

to the transport mechanism in PNA than in DNA, and we will address the implications for the charge transport below.

In addition to differences in coupling pathways for PNA and DNA, the MD simulations reveal structural differences among the duplexes that can affect the electrode-molecule electronic couplings (γ_L and γ_R). Recall that V_T as well as γ_L and γ_R determine the electronic coupling interactions near the chain ends. The orientation of the terminal AT base pair, which contains the amine groups that bind to the Au electrodes, with respect to the first GC base pair of the G-block (see Figure 1) appears to be different in the PNA junctions than in the DNA duplexes. In particular, the DNA terminal base pairs exhibit larger structural fluctuations than in PNA, which leads to ‘fraying’ of the duplex in the absence of the distance constraint described above. In addition, the increased rigidity of the PNA nucleobases, which correlates with enhanced π - π stacking interactions, likely contributes to establishing strong contacts with the leads and increasing the conductance.

PNA vs DNA conductance

The average experimentally measured single-molecule length-dependent conductance for the high-conductance mode of each duplex is shown in Figure 4. For the N-to-N linked PNA, the average conductance of the highest conductance mode is $\sim 3 \times 10^{-2} G/G_0$ (where G_0 is the quantum of conductance). The average conductances for the PNA duplexes are an order of magnitude larger (or more) than for DNA duplexes of the same length. Figure 4b shows the mean conductance value obtained from the PNA conductance histograms, which are 3-5 times larger than the literature conductance values reported for 3' DNA. In addition to the PNA conductances, the conductances for the first few ($n = 3, 4$, and 5) 3'- and 5'-linked G-block DNA duplexes were measured in this study and are plotted as filled symbols in Figure 4. The measurements performed

here are in good agreement with those reported by Tao and coworkers (unfilled symbols) and also display the even-odd oscillation.³⁰ Note that the increased conductance in PNA compared to DNA is consistent with earlier findings for mixed PNA sequences,^{29, 36} although the details of the mechanism for the large PNA conductance may be different.

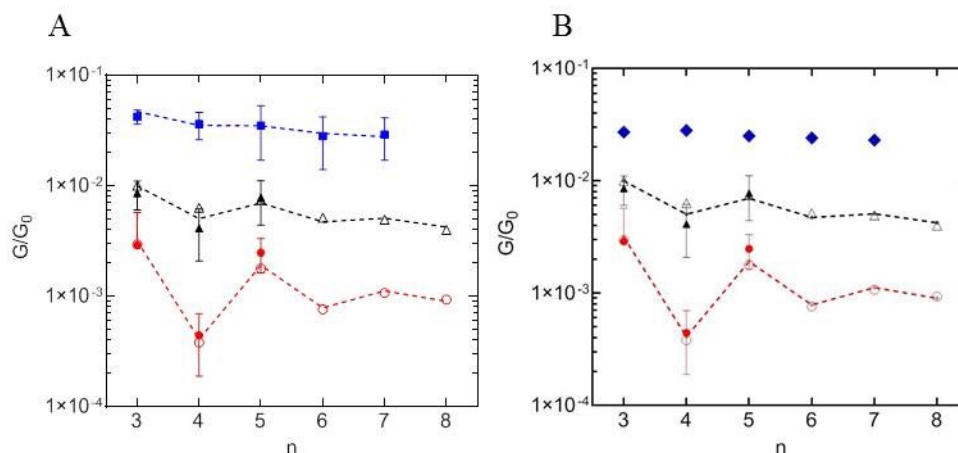


Figure 4. Panel A shows the results for the N linker PNA (blue squares) with data for 3'-linker DNA (black triangles) and 5'-linker DNA (red circles); the open symbols are from a previous study³⁰ and the filled symbols are from this study. Error bars are shown for the duplexes studied here representing a single standard deviation of the fitted Gaussian function for the highest observable mode. The negative component of the error for the 5'-linker DNA $n = 3$ data point has been excluded for clarity. The lines in the plot connect the best fit conductances found using the Büttiker double barrier model (see Supporting Information). Panel B shows an alternate analysis in which the PNA conductance values were assigned to the mean conductance value of the histogram, in order to show the increased PNA conduction in a model-independent manner.

The G-block PNA molecules show a significantly higher conductance (2 to 4 percent of G_0) than is typically found for molecules of comparable length, ~ 3 to 5 nm.⁷⁰ For example, molecules that display conductances on the order of a few percent of G_0 are typically the size of a single aromatic ring, e.g., benzenedithiol and benzenediamine. Two key factors influencing the molecular conductance in a junction are the electrode-molecule linker group and the molecule's electronic structure. The linker group can have an order(s) of magnitude effects on the measured conductance.^{70, 71} The amine linkers for the PNA and DNA duplexes used in this study couple the aromatic stack of the duplex more strongly to the electrode than do the backbone-based thiol

linkers used in earlier studies.⁷² The electronic structure of the mediating molecule, e.g., saturated versus unsaturated, is known to have a large influence on the molecular conductance as well.⁶⁸ However, molecules with highly conjugated electronic structures, such as oligo(phenylene-vinylenes) and oligophenylethynylenes, show conductances in the range of $10^{-3} G_0$ or lower if they are a few nanometers in length.^{70, 73} The length dependence of the molecular conductance through a homologous series of molecules is often characterized using an exponential decay as a function of length L ; i.e., $\exp(-\beta L)$.⁷⁴ Conjugated molecules show a much weaker decay with distance (smaller β value) than do saturated systems. Both the shallow dependence of the PNA conductances on length and the high conductance values are consistent with transport mediated by extended π systems.

The observation that the molecular conductance of G-block PNA duplexes are 10 to 20 times higher than the corresponding 5'-DNA duplexes with the π -stacked linkers is consistent with previous observations. Bruot et al.⁷² compared the molecular conductance through 5'-A(CG)_nT-3' ($n = 2-12$) DNA duplexes consisting of thiol linker groups connecting to the nucleic acid backbone with duplexes of the identical nucleobase sequence that have amine linkers bonded directly to the base stack. They found that the conductance was 10-20 times higher for the π -stack linker than the backbone linker for otherwise identical DNA duplexes. In earlier studies, we compared the molecular conductance of PNA duplexes to DNA duplexes with thiol linker groups on the nucleic acid backbone. In those cases, the PNA displayed a molecular conductance that was about 20 times higher than that of the DNA.^{29, 36} The high conductances measured for the PNA duplexes in this study is consistent with these earlier findings. The combined effects of the amine/thymine-based linker group and the high electronic coupling through the G-block stack are responsible for the high conductances reported here (vide infra).

Molecular orbital interpretation of conductance oscillations

The N-to-N linked PNA duplexes show a one- to two-order of magnitude increase in the molecular conductance compared to the values for the corresponding 5'-linked DNAs. This increase in conductance is consistent with the findings for mixed sequence DNA and PNA duplexes reported earlier.^{29, 36} Conductance oscillations observed previously in the 5'-linked and 3'-linked DNA systems are barely evident for the PNA duplexes. The decreased amplitude of the even-odd oscillations with G-block length is explained by the larger cross-strand coupling and electrode-molecule couplings in PNA.-We first discuss the cross-strand coupling effect and then examine the influence of the electrode-molecule coupling on the conductance oscillations.

In earlier studies, conductance oscillations as a function of length in G-block DNA duplexes (see Figure 4) were explained by an electronic energy effect that arises in finite length periodic structures.^{30, 75, 76} Odd-length G-blocks possess a “mid band” localized orbital with an energy near the Fermi level of the gold electrode, approximately equal to the energy of a G monomer.³⁰ This length-independent near degeneracy was proposed to strengthen coherent charge transport for odd-length chains by providing a flickering resonance coupling pathway across the entire duplex.³⁰ In contrast, the orbital energies for even length G-blocks are offset from the “mid-band” position (Figure 5) and are unlikely to form flickering resonance coupling pathways across the structures. This picture accounts for the conductance oscillations with length, as shown in Figure 4.

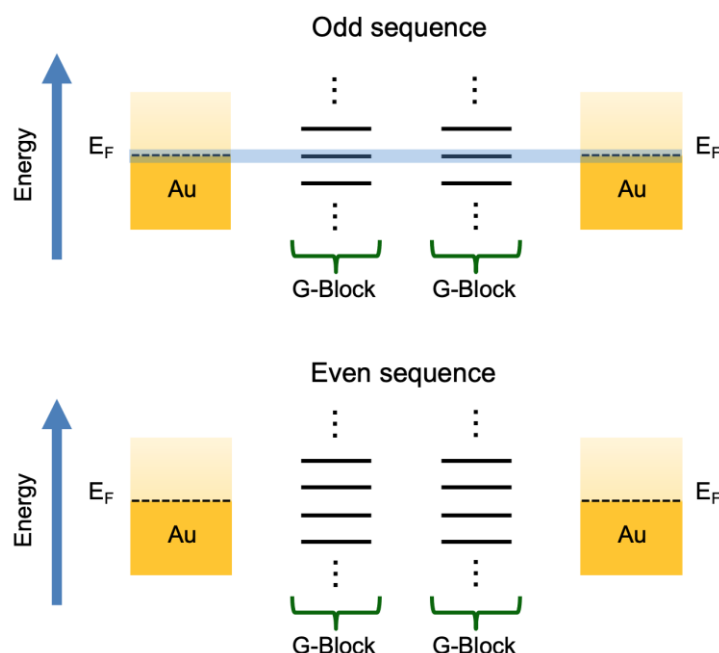


Figure 5. Molecular orbital energy picture of nucleic acid duplexes under a weak cross-strand coupling. **Top:** Flickering resonance energy level alignment for odd-length sequences. Each G-block possess a mid-band orbital in resonance with the Fermi level of the electrodes. **Bottom:** Energy level alignment for even sequences. A mid-band state in resonance with the Fermi level of the electrodes is absent.

Figure 4 shows that the conductance oscillations diminish in amplitude through the three duplex types as the overall conductance of the duplex increases. For example, the conductance oscillations are substantially less pronounced when the molecular linkers are positioned at the 3' termini of DNA, as compared to the 5' termini, and the corresponding molecular conductance of the 3' species is observed to be larger. The decrease in the amplitude of the conductance oscillations, and the overall increase in the conductance in DNA, was attributed to geometric differences of the base pairs at the cross-strand position in the two cases (Figure S7 and Figure S8), which causes a change in the cross-strand coupling.³⁰ Intriguingly, a large cross-strand GC-GC coupling at the molecule's center reduces the likelihood of forming a fully delocalized (resonant) state across the G-blocks and the electrodes (*vide infra*).⁷⁷

As a rule of thumb, the number of G bases over which the hole can delocalize at room temperature is up to about five.^{30, 78} When the cross-strand coupling is weak, as in DNA 5', the

dominant position for the delocalized hole is across the n guanines that form each of the separate G-blocks, forming two domains. Thermal fluctuations can bring these two domains into resonance, i.e., flickering resonance, and form a fully delocalized state across the entire duplex³⁷ (Figure 6). Because the odd length G-blocks have resonant states near the Fermi level, and the even length G-blocks do not, a strong modulation of the conductance with the G-block length is predicted to manifest. As the cross-strand coupling increases, delocalization can occur among G nucleobases of the two blocks, and this leads to a lower statistical weight for configurations that have the hole delocalized over each of the G-blocks. The growth in the number of configurations with delocalized domains leads to a higher overall conductance. The decreased statistical importance of the configuration with the extended G-block delocalization manifests as a decrease in the amplitude of the even-odd length conductance oscillations. Overall, the conductance is limited by the squared coupling between these domains and by the molecule-lead interaction strengths. The observation that the conductance increases from DNA 5', to DNA 3' - and increases further as the backbone is switched to PNA - is consistent with growth in the number and size of the cross-strand delocalization domains and their importance for the charge transport (switching from 5' to 3' increases the cross-strand coupling 3-4 fold, and switching to PNA increases the coupling by almost another 2 fold).

Figure 6 illustrates this mechanistic explanation for the change in conductance and in the even-odd effect for 5'-DNA and PNA. The bottom panel illustrates the mechanistic picture described in our prior analysis of the even/odd effects on the 5'-linked DNA conductance.³⁰ In this structure, the weaker cross-strand coupling in the 5' structure (compared to 3') leads to delocalization of orbitals on each of the two separated G blocks. Formation of a transient structure with extended delocalization only requires bringing these two blocks into resonance with each

other and with the electrodes. The figure illustrates the case of odd length ($n = 3$) and even length ($n = 4$) chains in order to underscore how the energy of the G-block states are offset from the Fermi level of the electrodes. The dependence of the energy mismatch on whether n is even or n is odd, and the promotion of delocalization across each G-block by the weak cross-strand coupling, leads to a strong even-odd conductance effect.

The top panel in Figure 6 explains the mechanistic picture for the case where the cross-strand coupling is large (comparable to the intra-strand GC-GC couplings). In this case, many possible delocalized islands of about five or fewer Gs may form in the structure. Indeed, in this regime, the likelihood of forming a delocalized state spread over the entire length of each G-block is diminished because of the increase in the overall number of other possible configurations that support delocalization, as illustrated by the additional two configurations shown in the top panel of Figure 6. Although this effect creates delocalized islands with more than one energy mismatch (so that multiple level matchings are required to delocalize over the entire molecule), many more configurations which display these delocalized islands manifest and provide many more flickering resonance conductance pathways in PNA, which leads to an overall increase in its conductance.

Our theoretical analysis (Table 3 and discussion) suggests that the electrode-molecule couplings for the PNA duplexes are stronger than in the 3'-linked and 5'-linked DNA. This feature is not included in the diagrams of Figure 6 for simplicity. A stronger electrode-molecule coupling is expected to produce a stronger mixing between the gold and the G-blocks of PNA compared to DNA. The stronger molecule-lead coupling expected to further enhance the conductance of PNA. This prediction is consistent with the observed higher conductance in PNA and softer even-odd effect compared to DNA. We note that strong molecule-lead interactions can perturb the "band structure" for each G-block, and will shift the energy of the mid-band state that appears for odd-

length chains. The effect of the strong molecule-lead coupling can break the degeneracy between delocalized hole states in each G-block and dampen the conductance oscillations in PNA compared to the case in 5'-DNA. This scenario was explored in detail by Segal et al., who showed that strong molecule-lead hybridization can indeed cause the even-odd effects to vanish.⁷⁵

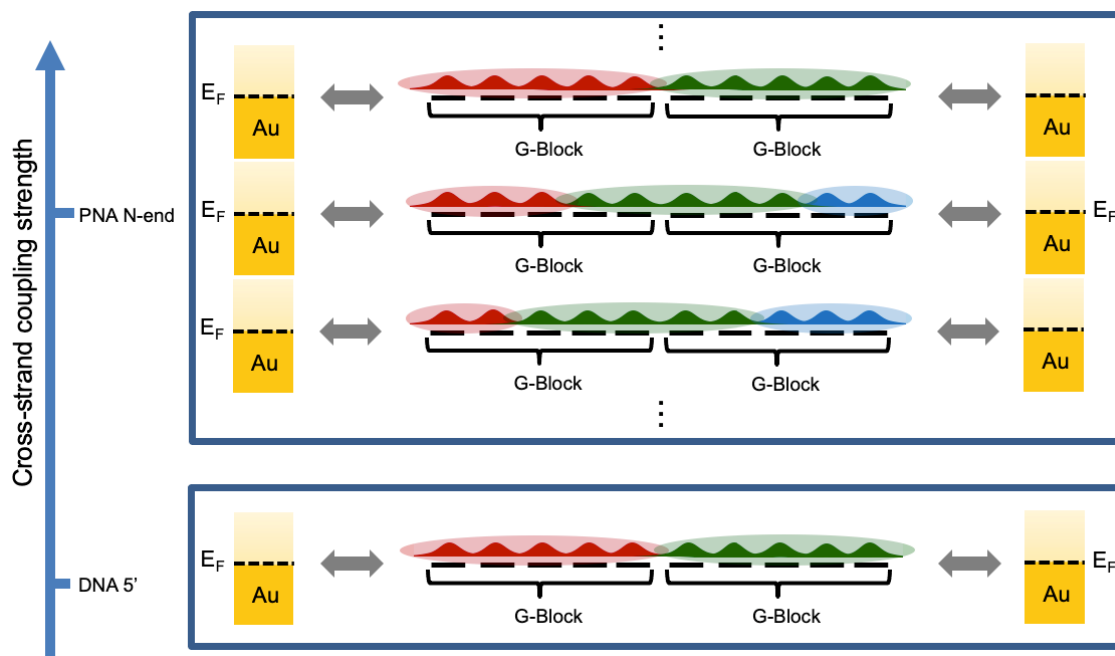


Figure 6. Model describing the delocalized islands across two G-blocks, each with $n = 5$. The maximum number of Gs over which the hole can delocalize is up to five (each color represents a delocalized block of orbitals).^{30, 78} **Top:** Regime with a strong cross-strand coupling. The strong cross-strand coupling allows the five base pair delocalization to occur anywhere across the entire ten-base sequence of the G-blocks (e.g., the green block can be delocalized across the two strands). Therefore, the carrier position in PNA is less constrained than in DNA. For the sake of illustration, three possible configurations that support delocalization are shown (many others are possible). **Bottom:** Regime where the coherent channel with the hole delocalized over each G-block contributes significantly to the conductance. This coherent channel is absent in even-length sequences (see Figure 5).^{30, 75} The weak cross-strand coupling pins the carrier delocalization on one of the G-blocks. The odd length G-block sequences are near resonant with the Fermi level of the leads and create a delocalized state for coherent transport.

CONCLUSIONS

Charge transport through nucleic acids can access coherent, incoherent, and flickering resonance mechanisms. The experimental and theoretical studies reported here find that structural differences in the duplex backbone with the same base sequences can produce order-of-magnitude

changes in molecular conductances and can strongly influence how coherence manifests for single-molecule PNA and DNA junctions. For PNA duplexes, a conductance value of $0.03 G_0$ was found with fourteen base pairs (~ 50 Å). PNA also has a high-mode conductance that is up to 30 times larger than that of DNA, and the conductance decreases monotonically with duplex length. The corresponding DNA structures show a striking conductance oscillation. The nearly monotonic and weak (< 2 -fold for distances from ~ 2 to 5 nm) change in conductance with duplex length that is found in PNA indicates an extremely low molecular resistance, in strong contrast with that for the 5'-linked DNA duplexes. The overall conductance in 5' DNA changes by only two-fold between the $n = 3$ and $n = 8$ G-block pairs. The even-odd conductance oscillations in 5' DNA with G-block length can be up to four-fold, and the average conductance in 5' DNA is one to two orders of magnitude lower than in PNA. Despite these dramatic differences in the experimental conductances and their length dependences, the flickering resonance transport mechanism provides a consistent explanation for the observed behavior.

Theoretical analysis finds that the PNA and DNA G-block structures studied here have similar structural flexibility, base-energy fluctuations, and base-to-base electronic interactions. The main differences between the PNA and DNA duplexes appear to be rooted in 1) differences in the molecule-electrode interaction strength and 2) differences in the base-to-base interactions in the cross-strand region, which arises from geometry differences between duplex PNA and DNA. The stronger cross-strand and molecule-lead couplings in PNA lead to higher conductance than in DNA. As such, the characteristics of cross-strand, intra-strand, and molecule-lead couplings collectively influence the contribution of competing coupling pathways to the conductance. The mechanistic origin of the even-odd conductance effect found in the DNA is consistent with that reported earlier,³⁰ which found that cross-strand interactions in the center of the duplex tips the

balance among mechanisms. In contrast to earlier studies, the findings reported here indicate that the conductance mechanism is also influenced by the strength of the nucleic acid-electrode interactions. Growing the electrode-molecule or the block-to-block couplings is expected to reduce the statistical importance of delocalized states spread across just one G-block, leads to a decrease in the even-odd length conductance oscillations with length, and produce an overall increase in the molecular conductance. Future work should explore effects of the molecule-lead coupling strength on conductance; for example, one can vary the aliphatic chain length of the amine linkers or modify the electrode's Fermi level in order to realize this goal. Detailed theoretical studies to assess the molecule-lead interactions⁷⁹ would also be incisive.

ACKNOWLEDGMENTS

This material is based upon work supported by the National Science Foundation (1412030 and 1900078 to D.H.W, 1413202 to C.A., and 1925690 to J.V., P.Z., and D.N.B. E.B. acknowledges a fellowship from the Pittsburgh Quantum Institute during part of this work. J.V. acknowledges support of a Fulbright-García Robles Scholarship and is grateful to Dr. Yuqi Zhang and Prof. Julio L. Palma for helpful discussions.

ASSOCIATED CONTENT

Supporting Information

The Supporting Information provides a description of control experiments for the STM break-junction measurements, details of DNA conductance measurements reported in Figure 3 and Figure 4, detailed MD procedures, RMSD plots, helical parameters, analysis of average structures from the MD production runs, HOMO energies of each base pair, and details of data fitting to eq 1.

REFERENCES

1. Genereux, J. C.; Barton, J. K., Mechanisms for DNA charge transport. *Chem. Rev.* **2010**, *110* (3), 1642-1662.

2. Lewis, F. D.; Young, R. M.; Wasielewski, M. R., Tracking photoinduced charge separation in DNA: from start to finish. *Acc. Chem. Res.* **2018**, *51* (8), 1746-1754.
3. Lewis, F. D.; Wu, T.; Zhang, Y.; Letsinger, R. L.; Greenfield, S. R.; Wasielewski, M. R., Distance-dependent electron transfer in DNA hairpins. *Science* **1997**, *277* (5326), 673-676.
4. Fink, H.-W.; Schönenberger, C., Electrical conduction through DNA molecules. *Nature* **1999**, *398* (6726), 407-410.
5. Kelley, S. O.; Jackson, N. M.; Hill, M. G.; Barton, J. K., Long-range electron transfer through DNA films. *Angew. Chem., Int. Ed.* **1999**, *38* (7), 941-945.
6. Giese, B.; Amaudrut, J.; Köhler, A.-K.; Spormann, M.; Wessely, S., Direct observation of hole transfer through DNA by hopping between adenine bases and by tunnelling. *Nature* **2001**, *412* (6844), 318-320.
7. Xu, B.; Zhang, P.; Li, X.; Tao, N., Direct conductance measurement of single DNA molecules in aqueous solution. *Nano Lett.* **2004**, *4* (6), 1105-1108.
8. Risser, S. M.; Beratan, D. N.; Meade, T. J., Electron transfer in DNA: predictions of exponential growth and decay of coupling with donor-acceptor distance. *J. Am. Chem. Soc.* **1993**, *115* (6), 2508-2510.
9. Jortner, J.; Bixon, M.; Langenbacher, T.; Michel-Beyerle, M. E., Charge transfer and transport in DNA. *Proc. Natl. Acad. Sci.* **1998**, *95* (22), 12759-12765.
10. Renaud, N.; Berlin, Y. A.; Lewis, F. D.; Ratner, M. A., Between superexchange and hopping: An intermediate charge-transfer mechanism in poly (A)-poly (T) DNA hairpins. *J. Am. Chem. Soc.* **2013**, *135* (10), 3953-3963.
11. Beratan, D. N., Why are DNA and protein electron transfer so different? *Annu. Rev. Phys. Chem.* **2019**, *70*, 71-97.
12. Beratan, D. N.; Liu, C.; Migliore, A.; Polizzi, N. F.; Skourtis, S. S.; Zhang, P.; Zhang, Y., Charge transfer in dynamical biosystems, or the treachery of (static) images. *Acc. Chem. Res.* **2015**, *48* (2), 474-481.
13. Korol, R.; Segal, D., From exhaustive simulations to key principles in DNA nanoelectronics. *J. Phys. Chem. C* **2018**, *122* (8), 4206-4216.
14. Beratan, D. N.; Priyadarshy, S.; Risser, S. M., DNA: insulator or wire? *Chem. Biol.* **1997**, *4* (1), 3-8.
15. Priyadarshy, S.; Risser, S.; Beratan, D., DNA is not a molecular wire: protein-like electron-transfer predicted for an extended π -electron system. *J. Phys. Chem.* **1996**, *100* (44), 17678-17682.
16. Teo, R. D.; Rousseau, B. J.; Smithwick, E. R.; Di Felice, R.; Beratan, D. N.; Migliore, A., Charge transfer between [4Fe4S] proteins and DNA is unidirectional: Implications for biomolecular signaling. *Chem* **2019**, *5* (1), 122-137.
17. Kilgour, M.; Segal, D., Charge transport in molecular junctions: From tunneling to hopping with the probe technique. *J. Chem. Phys.* **2015**, *143* (2), 024111.
18. Berlin, Y. A.; Burin, A. L.; Ratner, M. A., Charge hopping in DNA. *J. Am. Chem. Soc.* **2001**, *123* (2), 260-268.
19. Berlin, Y. A.; Kurnikov, I. V.; Beratan, D.; Ratner, M. A.; Burin, A. L., DNA electron transfer processes: Some theoretical notions. In *Long-Range Charge Transfer in DNA II*, Schuster, G. B., Ed. Springer: Berlin, 2004; pp 1-36.
20. Venkatramani, R.; Davis, K. L.; Wierzbinski, E.; Bezer, S.; Balaeff, A.; Keinan, S.; Paul, A.; Kocsis, L.; Beratan, D. N.; Achim, C., Evidence for a near-resonant charge transfer mechanism for double-stranded peptide nucleic acid. *J. Am. Chem. Soc.* **2011**, *133* (1), 62-72.

21. Xiang, L.; Palma, J. L.; Bruot, C.; Mujica, V.; Ratner, M. A.; Tao, N., Intermediate tunnelling–hopping regime in DNA charge transport. *Nat. Chem.* **2015**, 7 (3), 221.
22. Michaeli, K.; Beratan, D. N.; Waldeck, D. H.; Naaman, R., Voltage-induced long-range coherent electron transfer through organic molecules. *Proc. Natl. Acad. Sci.* **2019**, 116 (13), 5931-5936.
23. Buttiker, M., Coherent and sequential tunneling in series barriers. *IBM J. Res. Dev.* **1988**, 32 (1), 63-75.
24. Di Felice, R.; Calzolari, A.; Molinari, E.; Garbesi, A., Ab initio study of model guanine assemblies: The role of π – π coupling and band transport. *Phys. Rev. B* **2001**, 65 (4), 045104.
25. Livshits, G. I.; Stern, A.; Rotem, D.; Borovok, N.; Eidelstein, G.; Migliore, A.; Penzo, E.; Wind, S. J.; Di Felice, R.; Skourtis, S. S., Long-range charge transport in single G-quadruplex DNA molecules. *Nat. Nanotechnol.* **2014**, 9 (12), 1040.
26. Wierzbinski, E.; Venkatramani, R.; Davis, K. L.; Bezer, S.; Kong, J.; Xing, Y.; Borguet, E.; Achim, C.; Beratan, D. N.; Waldeck, D. H., The single-molecule conductance and electrochemical electron-transfer rate are related by a power law. *ACS Nano* **2013**, 7 (6), 5391-5401.
27. Wolak, M. u. A.; Balaeff, A.; Gutmann, S.; Helmrigh, H. J.; Vosloo, R.; Beerbom, M. M.; Wierzbinski, E.; Waldeck, D. H.; Bezer, S.; Achim, C., Electronic structure of self-assembled peptide nucleic acid thin films. *J. Phys. Chem. C* **2011**, 115 (34), 17123-17135.
28. Paul, A.; Bezer, S.; Venkatramani, R.; Kocsis, L.; Wierzbinski, E.; Balaeff, A.; Keinan, S.; Beratan, D. N.; Achim, C.; Waldeck, D. H., Role of nucleobase energetics and nucleobase interactions in single-stranded peptide nucleic acid charge transfer. *J. Am. Chem. Soc.* **2009**, 131 (18), 6498-6507.
29. Beall, E.; Sargun, A.; Ulku, S.; Bae, Y.; Wierzbinski, E.; Clever, C.; Waldeck, D. H.; Achim, C., Molecular conductance of nicked nucleic acid duplexes. *J. Phys. Chem. C* **2018**, 122 (13), 7533-7540.
30. Liu, C.; Xiang, L.; Zhang, Y.; Zhang, P.; Beratan, D. N.; Li, Y.; Tao, N., Engineering nanometre-scale coherence in soft matter. *Nat. Chem.* **2016**, 8 (10), 941-945.
31. Šponer, J.; Leszczyński, J.; Hobza, P., Nature of nucleic acid– base stacking: nonempirical ab initio and empirical potential characterization of 10 stacked base dimers. Comparison of stacked and H-bonded base pairs. *J. Phys. Chem.* **1996**, 100 (13), 5590-5596.
32. Voityuk, A. A., Electronic couplings and on-site energies for hole transfer in DNA: Systematic quantum mechanical/molecular dynamic study. *J. Chem. Phys.* **2008**, 128 (11), 03B608.
33. Hatcher, E.; Balaeff, A.; Keinan, S.; Venkatramani, R.; Beratan, D. N., PNA versus DNA: Effects of structural fluctuations on electronic structure and hole-transport mechanisms. *J. Am. Chem. Soc.* **2008**, 130 (35), 11752-11761.
34. Venkatramani, R.; Keinan, S.; Balaeff, A.; Beratan, D. N., Nucleic acid charge transfer: black, white and gray. *Coord. Chem. Rev.* **2011**, 255 (7-8), 635-648.
35. Wierzbinski, E.; de Leon, A.; Yin, X.; Balaeff, A.; Davis, K. L.; Reppireddy, S.; Venkatramani, R.; Keinan, S.; Ly, D. H.; Madrid, M., Effect of backbone flexibility on charge transfer rates in peptide nucleic acid duplexes. *J. Am. Chem. Soc.* **2012**, 134 (22), 9335-9342.
36. Beall, E.; Ulku, S.; Liu, C.; Wierzbinski, E.; Zhang, Y.; Bae, Y.; Zhang, P.; Achim, C.; Beratan, D. N.; Waldeck, D. H., Effects of the backbone and chemical linker on the molecular conductance of nucleic acid duplexes. *J. Am. Chem. Soc.* **2017**, 139 (19), 6726-6735.

37. Zhang, Y.; Liu, C.; Balaeff, A.; Skourtis, S. S.; Beratan, D. N., Biological charge transfer via flickering resonance. *Proc. Natl. Acad. Sci.* **2014**, *111* (28), 10049-10054.
38. Egholm, M.; Buchardt, O.; Christensen, L.; Behrens, C.; Freier, S. M.; Driver, D. A.; Berg, R. H.; Kim, S. K.; Norden, B.; Nielsen, P. E., PNA hybridizes to complementary oligonucleotides obeying the Watson–Crick hydrogen-bonding rules. *Nature* **1993**, *365* (6446), 566-568.
39. Xu, B.; Tao, N. J., Measurement of single-molecule resistance by repeated formation of molecular junctions. *Science* **2003**, *301* (5637), 1221-1223.
40. Beall, E.; Yin, X.; Waldeck, D. H.; Wierzbinski, E., A scanning tunneling microscope break junction method with continuous bias modulation. *Nanoscale* **2015**, *7* (36), 14965-14973.
41. Van Wees, B.; Van Houten, H.; Beenakker, C.; Williamson, J. G.; Kouwenhoven, L.; Van der Marel, D.; Foxon, C., Quantized conductance of point contacts in a two-dimensional electron gas. *Phys. Rev. Lett.* **1988**, *60* (9), 848.
42. Afsari, S.; Li, Z.; Borguet, E., Orientation-Controlled Single-Molecule Junctions. *Angew. Chem., Int. Ed.* **2014**, *53* (37), 9771-9774.
43. Komoto, Y.; Fujii, S.; Nishino, T.; Kiguchi, M., High electronic couplings of single mesitylene molecular junctions. *Beilstein J. Nanotechnol.* **2015**, *6* (1), 2431-2437.
44. Hanwell, M. D.; Curtis, D. E.; Lonie, D. C.; Vandermeersch, T.; Zurek, E.; Hutchison, G. R., Avogadro: an advanced semantic chemical editor, visualization, and analysis platform. *J. Cheminf.* **2012**, *4* (1), 17.
45. Schrödinger Release 2019-4: Maestro, *Schrödinger, LLC, New York, NY, 2019*.
46. Yeh, J. I.; Pohl, E.; Truan, D.; He, W.; Sheldrick, G. M.; Du, S.; Achim, C., The Crystal Structure of Non-Modified and Bipyridine-Modified PNA Duplexes. *Chem. Eur. J.* **2010**, *16* (39), 11867-11875.
47. Hart, K.; Foloppe, N.; Baker, C. M.; Denning, E. J.; Nilsson, L.; MacKerell Jr, A. D., Optimization of the CHARMM additive force field for DNA: Improved treatment of the BI/BII conformational equilibrium. *J. Chem. Theory Comput.* **2012**, *8* (1), 348-362.
48. Jasiński, M.; Feig, M.; Trylska, J., Improved force fields for peptide nucleic acids with optimized backbone torsion parameters. *J. Chem. Theory Comput.* **2018**, *14* (7), 3603-3620.
49. Jorgensen, W. L.; Chandrasekhar, J.; Madura, J. D.; Impey, R. W.; Klein, M. L., Comparison of simple potential functions for simulating liquid water. *J. Chem. Phys.* **1983**, *79* (2), 926-935.
50. Zgarbová, M.; Otyepka, M.; Sponer, J.; Lankas, F.; Jurečka, P., Base pair fraying in molecular dynamics simulations of DNA and RNA. *J. Chem. Theory Comput.* **2014**, *10* (8), 3177-3189.
51. Phillips, J. C.; Braun, R.; Wang, W.; Gumbart, J.; Tajkhorshid, E.; Villa, E.; Chipot, C.; Skeel, R. D.; Kale, L.; Schulten, K., Scalable molecular dynamics with NAMD. *J. Comput. Chem.* **2005**, *26* (16), 1781-1802.
52. Pacher, T.; Cederbaum, L.; Köppel, H., Approximately diabatic states from block diagonalization of the electronic Hamiltonian. *J. Chem. Phys.* **1988**, *89* (12), 7367-7381.
53. Ridley, J.; Zerner, M., An intermediate neglect of differential overlap technique for spectroscopy: pyrrole and the azines. *Theor. Chim. Acta* **1973**, *32* (2), 111-134.
54. Zeng, J.; Hush, N.; Reimers, J., Solvent effects on molecular and ionic spectra. 7. Modeling the absorption and electroabsorption spectra of pentaammine-ruthenium (II) pyrazine and its conjugate acid in water. *J. Am. Chem. Soc.* **1996**, *118* (8), 2059-2068.

55. Voityuk, A. A., Assessment of semiempirical methods for the computation of charge transfer in DNA π -stacks. *Chem. Phys. Lett.* **2006**, *427* (1-3), 177-180.
56. Kubař, T.; Elstner, M., What governs the charge transfer in DNA? The role of DNA conformation and environment. *J. Phys. Chem. B* **2008**, *112* (29), 8788-8798.
57. Kubař, T.; Kleinekathöfer, U.; Elstner, M., Solvent fluctuations drive the hole transfer in DNA: a mixed quantum– classical study. *J. Phys. Chem. B* **2009**, *113* (39), 13107-13117.
58. Boese, A. D., Density functional theory and hydrogen bonds: are we there yet? *ChemPhysChem* **2015**, *16* (5), 978-985.
59. Peverati, R.; Truhlar, D. G., Improving the accuracy of hybrid meta-GGA density functionals by range separation. *J. Phys. Chem. Lett.* **2011**, *2* (21), 2810-2817.
60. Zheng, J.; Xu, X.; Truhlar, D. G., Minimally augmented Karlsruhe basis sets. *Theor. Chem. Acc.* **2011**, *128* (3), 295-305.
61. Frisch, M. J. T.; G. W.; Schlegel, H. B.; Scuseria, G. E.; Robb, M. A.; Cheeseman, J. R.; Scalmani, G.; Barone, V.; Petersson, G. A.; Nakatsuji, H.; Li, X.; Caricato, M.; Marenich, A. V.; Bloino, J.; Janesko, B. G.; Gomperts, R.; Mennucci, B.; Hratchian, H. P.; Ortiz, J. V.; Izmaylov, A. F.; Sonnenberg, J. L.; Williams-Young, D.; Ding, F.; Lipparini, F.; Egidi, F.; Goings, J.; Peng, B.; Petrone, A.; Henderson, T.; Ranasinghe, D.; Zakrzewski, V. G.; Gao, J.; Rega, N.; Zheng, G.; Liang, W.; Hada, M.; Ehara, M.; Toyota, K.; Fukuda, R.; Hasegawa, J.; Ishida, M.; Nakajima, T.; Honda, Y.; Kitao, O.; Nakai, H.; Vreven, T.; Throssell, K.; Montgomery, J. A., Jr.; Peralta, J. E.; Ogliaro, F.; Bearpark, M. J.; Heyd, J. J.; Brothers, E. N.; Kudin, K. N.; Staroverov, V. N.; Keith, T. A.; Kobayashi, R.; Normand, J.; Raghavachari, K.; Rendell, A. P.; Burant, J. C.; Iyengar, S. S.; Tomasi, J.; Cossi, M.; Millam, J. M.; Klene, M.; Adamo, C.; Cammi, R.; Ochterski, J. W.; Martin, R. L.; Morokuma, K.; Farkas, O.; Foresman, J. B.; Fox, D. J., *Gaussian 16, Revision B. 01, Gaussian Inc., Wallingford CT, 2016*.
62. Li, C.; Pobelov, I.; Wandlowski, T.; Bagrets, A.; Arnold, A.; Evers, F., Charge transport in single Au| alkanedithiol| Au junctions: coordination geometries and conformational degrees of freedom. *J. Am. Chem. Soc.* **2008**, *130* (1), 318-326.
63. Haiss, W.; Martín, S.; Leary, E.; Zalinge, H. v.; Higgins, S. J.; Bouffier, L.; Nichols, R. J., Impact of junction formation method and surface roughness on single molecule conductance. *J. Phys. Chem. C* **2009**, *113* (14), 5823-5833.
64. Humphrey, W.; Dalke, A.; Schulten, K., VMD: visual molecular dynamics. *J. Mol. Graphics* **1996**, *14* (1), 33-38.
65. Tan, B.; Hodak, M.; Lu, W.; Bernholc, J., Charge transport in DNA nanowires connected to carbon nanotubes. *Phys. Rev. B* **2015**, *92* (7), 075429.
66. Neaton, J. B.; Hybertsen, M. S.; Louie, S. G., Renormalization of molecular electronic levels at metal-molecule interfaces. *Phys. Rev. Lett.* **2006**, *97* (21), 216405.
67. Teo, R. D.; Terai, K.; Migliore, A.; Beratan, D. N., Electron transfer characteristics of 2'-deoxy-2'-fluoro-arabinonucleic acid, a nucleic acid with enhanced chemical stability. *Phys. Chem. Chem. Phys.* **2018**, *20* (41), 26063-26067.
68. Roca-Sanjuán, D.; Rubio, M.; Merchán, M.; Serrano-Andrés, L., Ab initio determination of the ionization potentials of DNA and RNA nucleobases. *J. Chem. Phys.* **2006**, *125* (8), 084302.
69. Kawai, K.; Majima, T., Hole transfer kinetics of DNA. *Acc. Chem. Res.* **2013**, *46* (11), 2616-2625.
70. Evers, F.; Korytár, R.; Tewari, S.; van Ruitenbeek, J. M., Advances and challenges in single-molecule electron transport. *Rev. Mod. Phys.* **2020**, *92* (3), 035001.

71. Tivanski, A. V.; He, Y.; Borguet, E.; Liu, H.; Walker, G. C.; Waldeck, D. H., Conjugated thiol linker for enhanced electrical conduction of gold– molecule contacts. *J. Phys. Chem. B* **2005**, *109* (12), 5398-5402.
72. Bruot, C.; Xiang, L.; Palma, J. L.; Tao, N., Effect of mechanical stretching on DNA conductance. *ACS Nano* **2015**, *9* (1), 88-94.
73. Frisenda, R.; Stefani, D.; van der Zant, H. S., Quantum transport through a single conjugated rigid molecule, a mechanical break junction study. *Acc. Chem. Res.* **2018**, *51* (6), 1359-1367.
74. Valdiviezo, J.; Rocha, P.; Polakovsky, A.; Palma, J. L., Nonexponential Length Dependence of Molecular Conductance in Acene-Based Molecular Wires. *ACS Sens.* **2021**, *6* (2), 477-484.
75. Kim, H.; Kilgour, M.; Segal, D., Intermediate Coherent–Incoherent Charge Transport: DNA as a Case Study. *J. Phys. Chem. C* **2016**, *120* (42), 23951-23962.
76. Karasch, P.; Ryndyk, D. A.; Frauenheim, T., Vibronic dephasing model for coherent-to-incoherent crossover in DNA. *Phys. Rev. B* **2018**, *97* (19), 195401.
77. Carey, R.; Chen, L.; Gu, B.; Franco, I., When can time-dependent currents be reproduced by the Landauer steady-state approximation? *J. Chem. Phys.* **2017**, *146* (17), 174101.
78. Jin, Y.; Ru, X.; Su, N. Q.; Mei, Y.; Beratan, D. N.; Zhang, P.; Yang, W., Revisiting the Hole Size in Double Helical DNA with Localized Orbital Scaling Corrections. *J. Phys. Chem. B* **2020**, *124* (16), 3428-3435.
79. Bag, S.; Biswas, T.; Jain, M.; Maiti, P. K., Anisotropic Charge Transport in Nanoscale DNA Wire. *J. Phys. Chem. C* **2020**, *124* (31), 16763-16772.

TOC

